Satellite remote sensing of blowing snow properties over Antarctica

Stephen P. Palm,[1] Yuekui Yang,[2] James D. Spinhirne,[3] and Alexander Marshak[4]

Received 18 February 2011; revised 5 May 2011; accepted 24 May 2011; published 30 August 2011.

[1] A new technique for the detection of blowing snow events using satellite lidar data is applied to Cloud-Aerosol LIdar with Orthogonal Polarization (CALIOP) observations to obtain the spatial and temporal frequency, layer height, and optical depth of blowing snow events over Antarctica for 2007 through 2009. In addition, spatially and temporally collocated multichannel Moderate resolution Imaging Spectroradiometer (MODIS) data are utilized for the detection of two blowing snow events in sunlight. Blowing snow frequency as high as 70% is found to occur in some regions of Antarctica during winter. The spatial distribution of blowing snow closely follows the katabatic wind pattern with the exception of an area in East Antarctica that encompasses the megadune region, where the most persistent and largest area of blowing snow occurs. Layer thickness ranges from the minimum detectable (30 m) to about 1000 m with an average depth of 120 m for all blowing snow events. The layer optical depth estimated from the lidar data ranged from 0.05 to 1.0 with an average of 0.20. A very large, organized blowing snow "storm" is tracked over 3 days and is estimated to transport a mass of 6.3×10^3 kg m^{-1} d^{-1} which is comparable to surface-based measurements of mass transport during blowing snow events. Results from the application of the retrieval technique to ICESat data are also presented with a demonstration of the large multiple scattering-induced elevation error that blowing snow layers can cause.

Citation: Palm, S. P., Y. Yang, J. D. Spinhirne, and A. Marshak (2011), Satellite remote sensing of blowing snow properties over Antarctica, *J. Geophys. Res.*, *116*, D16123, doi:10.1029/2011JD015828.

1. Introduction

[2] The uplift and horizontal transport of snow by wind, heretofore referred to as blowing snow, occurs frequently in polar regions and continental midlatitude areas in winter. Blowing snow can quickly reduce visibility to near zero, thereby adversely affecting transportation and nearly all aspects of life in populated areas. In addition to its detrimental effects on society, blowing snow is important for a wide variety of reasons including ice sheet mass balance [*Gallée et al.*, 2001; *Déry and Yau*, 2002], the water budget of high-latitude regions [*Déry et al.*, 1998], and the reconstruction of paleoclimate records from the physical and chemical records obtained from ice cores [*King et al.*, 2004]. Interaction with blowing snow is a major factor for changes in surface ice characteristics, such as rifts, crevasses, ridges, sastrugi, etc. and in deposition of snow on sea ice [*Déry and Tremblay*, 2004; *Leonard et al.*, 2008; *Leonard and Maksym*, 2011]. For meteorology, blowing snow can also have important regional radiative and dynamic effects [*Mahesh et al.*, 2003; *Walden et al.*, 2003; *Lesins et al.*, 2009; *Yamanouchi and Kawaguchi*, 1985]. The presence of blowing snow is a concern for remote sensing of surface and atmospheric factors and will affect the retrieval of cloud and surface characteristics from passive observation. For laser altimetry measurements of ice sheets, in particular the ICESat (Ice Cloud and land Elevation Satellite) mission, it degrades the accuracy of measurements through multiple scattering pulse spreading which results in a time delay error of the laser pulse as it traverses through the blowing snow layer [*Duda et al.*, 2001; *Mahesh et al.*, 2002, *Yang et al.*, 2010].

[3] While many ground-based observations and modeling studies of blowing snow have provided valuable information such as particle size, number density, and the frequency of blowing snow events at a particular location [*Mann et al.*, 2000; *Nishimura and Nemoto*, 2005], the true extent and frequency of this phenomenon over the vast uninhabited regions of Antarctica remains largely unknown. The main reason for this is the scarcity of surface observations and the difficulty of passive satellite-borne sensors to unambiguously detect the presence of blowing snow. Passive remote sensing can be used to detect blowing snow provided that the surface is illuminated and clouds do not obscure the surface. *Scarchilli et al.* [2010] show dramatic examples of snow billows which are long linear features on visible MODerate resolution Imaging Spectroradiometer (MODIS) images over Terra Nova Bay, Antarctica. These billow features are aligned parallel with the

[1]Science Systems and Applications, Inc., Lanham, Maryland, USA.
[2]Universities Space Research Association, Columbia, Maryland, USA.
[3]Department of Electrical and Computer Engineering, University of Arizona, Tucson, Arizona, USA.
[4]Goddard Space Flight Center, Greenbelt, Maryland, USA.

Copyright 2011 by the American Geophysical Union.
0148-0227/11/2011JD015828

surface wind and separated by about 5 km, giving an appearance similar to cloud streets that often occur during cold air outbreaks and are seen in visible satellite images [*Brümmer*, 1999; *Renfrew and Moore*, 1999]. Further, *Scarchilli et al.* [2010] determined, by measuring the length of their shadows, that the height of the billows often reached 200 m.

[4] Ground-based measurement in Antarctica proved that blowing snow could be almost unambiguously detected and observed vertically from lidar (light detection and ranging) sensing [*Mahesh et al.*, 2003]. With the advent of active lidar remote sensing of the atmosphere from space via the ICESat in 2003 [*Spinhirne et al.*, 2005, *Palm et al.*, 2005] and later the Cloud-Aerosol Lidar and Infrared Pathfinder Satellite Observations (CALIPSO) satellite in 2006 [*Winker et al.*, 2007, 2009], comes the possibility of routinely detecting blowing snow over large regions, even during the dark of winter, something that is very difficult if not impossible to do with passive sensors. Blowing snow often occurs in thin layers only a few meters thick, but has occasionally been observed to reach heights of 100 m or more [*Mahesh et al.*, 2003; *Scarchilli et al.*, 2010; *Budd et al.*, 1966]. In such cases, it is easily detected by satellite lidar as long as scattering layers above the blowing snow do not fully attenuate the laser beam.

[5] This paper presents a technique for the detection of blowing snow events using satellite lidar data and demonstrates how satellite active and passive remote sensing can be used together to detect blowing snow episodes over Antarctica. More significantly, our application of the technique allows us to present properties of blowing snow including spatial and temporal frequency, height and optical depth, and an estimate of the mass transport involved in a large blowing snow outbreak. In section 2 we describe the algorithm that is used to detect blowing snow from satellite lidar data. In section 3 we discuss cases of blowing snow detection using ICESat data, while section 4 presents the synergistic use of CALIPSO and MODIS data for retrieval of blowing snow properties. In section 5 we briefly describe the validation of the blowing snow detection using surface observations, and in section 6 we present the detection and tracking of a large blowing snow "storm" and estimate the amount of mass being transported off the Antarctic continent by the katabatic winds. Section 7 presents the frequency analysis of 3 years of CALIPSO data showing the spatial and temporal distribution of blowing snow over Antarctica, and section 8 supplies a summary with concluding remarks. We begin with a brief description of the algorithm used to detect blowing snow layers using satellite lidar data in section 2.

2. Algorithm Description and Example

[6] The blowing snow detection algorithm uses as input the 5 Hz averaged, attenuated backscatter cross-section profiles from ICESat (GLA07 data product) and/or CALIPSO, a high-resolution (1 × 1 km) digital elevation model (DEM) and the 10 m wind speed obtained from the Goddard Earth Observing System 5 (GEOS-5) (CALIPSO products) and National Centers for Environmental Prediction (ICESat products) global numerical models. The backscatter profiles from both ICESat and CALIPSO extend from a roughly 40 km altitude to below sea level and take the form of vertical bins, 75 m wide in the case of ICESat and 30 m wide for CALIPSO (below 5 km altitude). Because of the finer vertical resolution, the CALIPSO data are better suited for the detection of thin layers, but as we shall see, ICESat is also able to detect the blowing snow layers. The blowing snow detection algorithm interrogates the lidar return bins directly above the ground for an elevated backscatter signal indicative of a scattering layer in contact with the ground. In order to accomplish this, it is imperative that the ground return bin be located so that it is certain that we are indeed looking at the bins immediately above the ground and that any contamination due to the ground signal itself be eliminated. The first step is to use the DEM available on both CALIPSO and ICESat products to define a 400 m wide window within which a search for the ground return is performed. The ground return is generally the strongest signal in the lidar backscattered return provided that overlying particulate layers have not strongly attenuated the laser beam. The ground search is performed from 200 m below the (DEM indicated) ground working upward in search of a signal exceeding the ground signal threshold (1.0 km^{-1} sr^{-1}). The ground threshold was determined empirically and represents a value attained when the atmospheric column two-way transmission is greater than about 10%. If the ground signal is found (call this bin "G"), and if the 10 m wind speed at the current location is greater than 4 m s^{-1} and the backscatter signal in the bin immediately above the ground (G-1) exceeds the blowing snow threshold (about 2.5×10^{-2} km^{-1} sr^{-1}), then a low-level, wind-induced "scattering layer" is assumed to be present.

[7] The blowing snow threshold is constructed from a scaling factor times the magnitude of 532 nm attenuated molecular (Rayleigh) scattering at the height of the current retrieval location. The scaling factor used for this analysis has a value of 20.0 and was determined by an iterative approach of adjustment and review of retrieval results until they were satisfactory. The resulting threshold must be great enough to ensure minimal false-positive detections but small enough to retain adequate sensitivity. The algorithm then interrogates the bins above (G-2, G-3, etc.) until the backscatter within the bin is less than the blowing snow threshold backscatter level times 0.20 (about 5.0×10^{-3} km^{-1} sr^{-1}). The top of the scattering layer is then the last bin to exceed this threshold. Once the layer is defined, the gradient of backscatter within the layer is computed. If the gradient decreases upward, then the layer is assumed to be blowing snow. Conversely, if the backscatter gradient increases upward, the layer is assumed to be low fog or cloud. This check, designed to eliminate low clouds, is done only if the layer is thicker than 1 bin.

[8] The output of the blowing snow detection algorithm has been extensively checked for consistency and quality by generating and reviewing hundreds of images of the detected blowing snow layers. A limitation of the lidar technique is that the blowing snow layer has to be at least 20 and 50 m thick in order for enough backscatter signal to be collected in the bin immediately above the ground by CALIPSO and ICESat, respectively. This means that shallow blowing snow layers, which may be frequent, will probably not be detected. Further, blowing snow cannot be detected beneath thick or highly attenuating layers (tropospheric or polar stratospheric clouds with optical depth more than ~1.5), since detection of a strong ground return is required. The latter

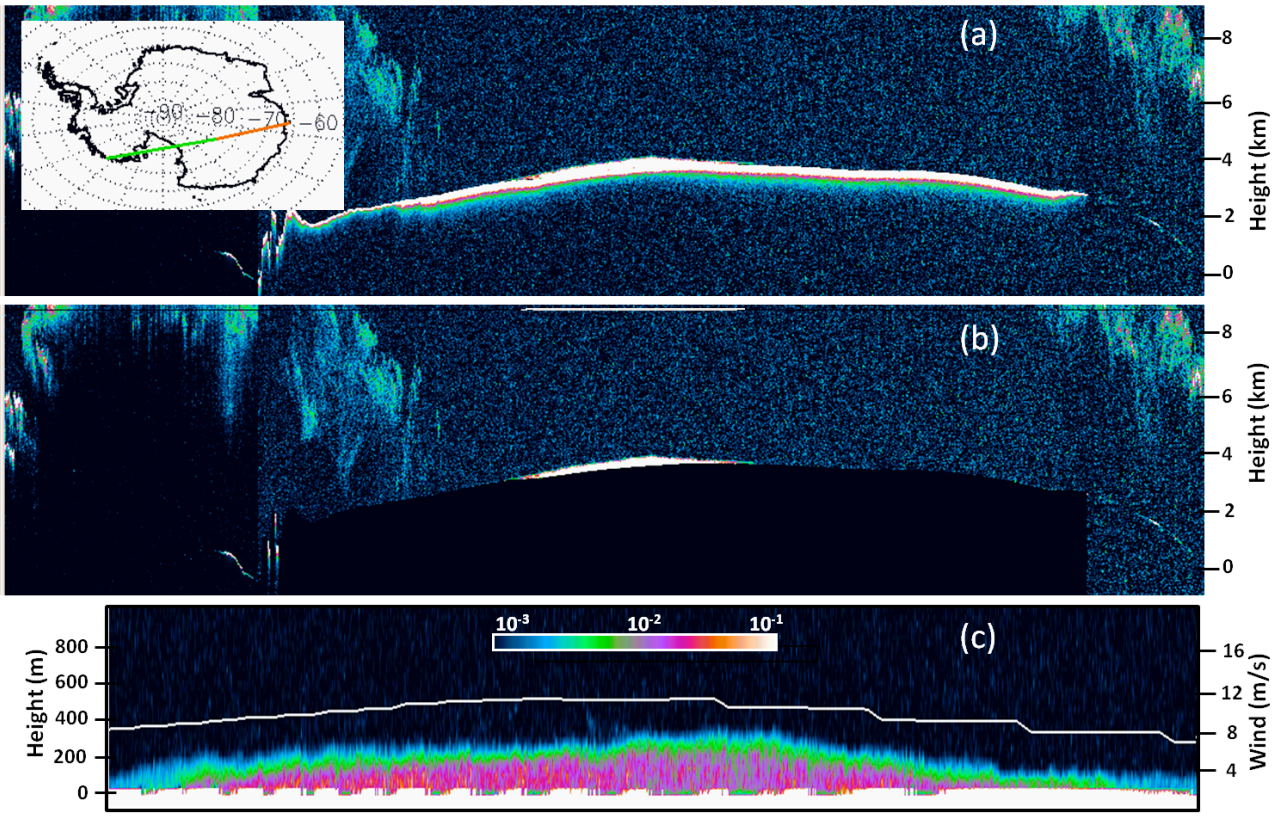

Figure 1. (a) CALIPSO attenuated backscatter for a segment over Antarctica (shown on the map) for 13 October 2009 and (b) the output of the blowing snow detection algorithm showing the location of the blowing snow (white line at the top of image) and (c) a blowup of the detected blowing snow layer. The color bar in Figure 1c shows the range of backscatter magnitude (km^{-1} sr^{-1}) within the blowing snow layer.

limitation implies that most of the blowing snow associated with winter storms (cyclones) will go undetected. These limitations will certainly result in lower blowing snow frequencies than actually exist. Furthermore, the magnitude of the discrepancy will depend on the cloud cover frequency of a given region. For instance, along the coast of Antarctica where blowing snow frequency is known to be high, it is also cloudier than more inland regions. Also, for the work presented here, the algorithm was "activated" only when the DEM value at the current latitude/longitude location of the satellite was above 50 m. This means that blowing snow retrieval was not attempted for areas surrounding the Antarctic landmass such as sea ice, ocean, or bay areas. We plan to address this issue separately in a future paper.

[9] An example of the output of the blowing snow detection algorithm is shown in Figure 1. Figure 1a is an image of CALIPSO 532 nm attenuated backscatter for a segment across Antarctica on 13 October 2009. The ground return is seen as the thick white line across the bottom portion of the image varying in altitude from 2 to 3 km. Notice that what appears to be the ground return is somewhat thicker in the middle portion of the image. This is because of the thin atmospheric scattering layer immediately adjacent to and in contact with the ground in this location. Figure 1b shows the same backscatter data, but now with the bins at or below the ground blacked out. Only the data in the above ground bins remain. The scattering layer is now immediately obvious, and the white line at the top of Figure 1b indicates the regions where blowing snow was detected by the algorithm. Figure 1c shows a zoomed-in view (and a change of the data scaling) of only the detected blowing snow layer (the white portion in Figure 1b). The layer extends up to 300 m at its thickest point with an average backscatter cross section of 0.1 km^{-1} sr^{-1} at 100 m altitude as seen by the color bar (the color bar pertains only to Figure 1c). The layer extends over 550 km in the horizontal and is typical of many that have been detected over Antarctica using both CALIPSO and ICESat data.

3. ICESat Measurements

[10] The blowing snow detection algorithm was developed and first implemented as part of the ICESat atmospheric data product software system that generates the ICESat data products in near real time [*Palm et al.*, 2002, *Spinhirne et al.*, 2005]. These products, which also include cloud and aerosol properties in addition to blowing snow detection (in the GLA09 product), are available at the National Snow and Ice Data Center in Boulder, Colorado. The original ICESat algorithm was later adapted for use with CALIPSO data, and most of the results presented herein are obtained using CALIPSO data. The main reason for this is the fact that CALIPSO has been acquiring data continuously since June 2006, while ICESat experienced laser problems that severely curtailed the amount of atmospheric data obtained. Also,

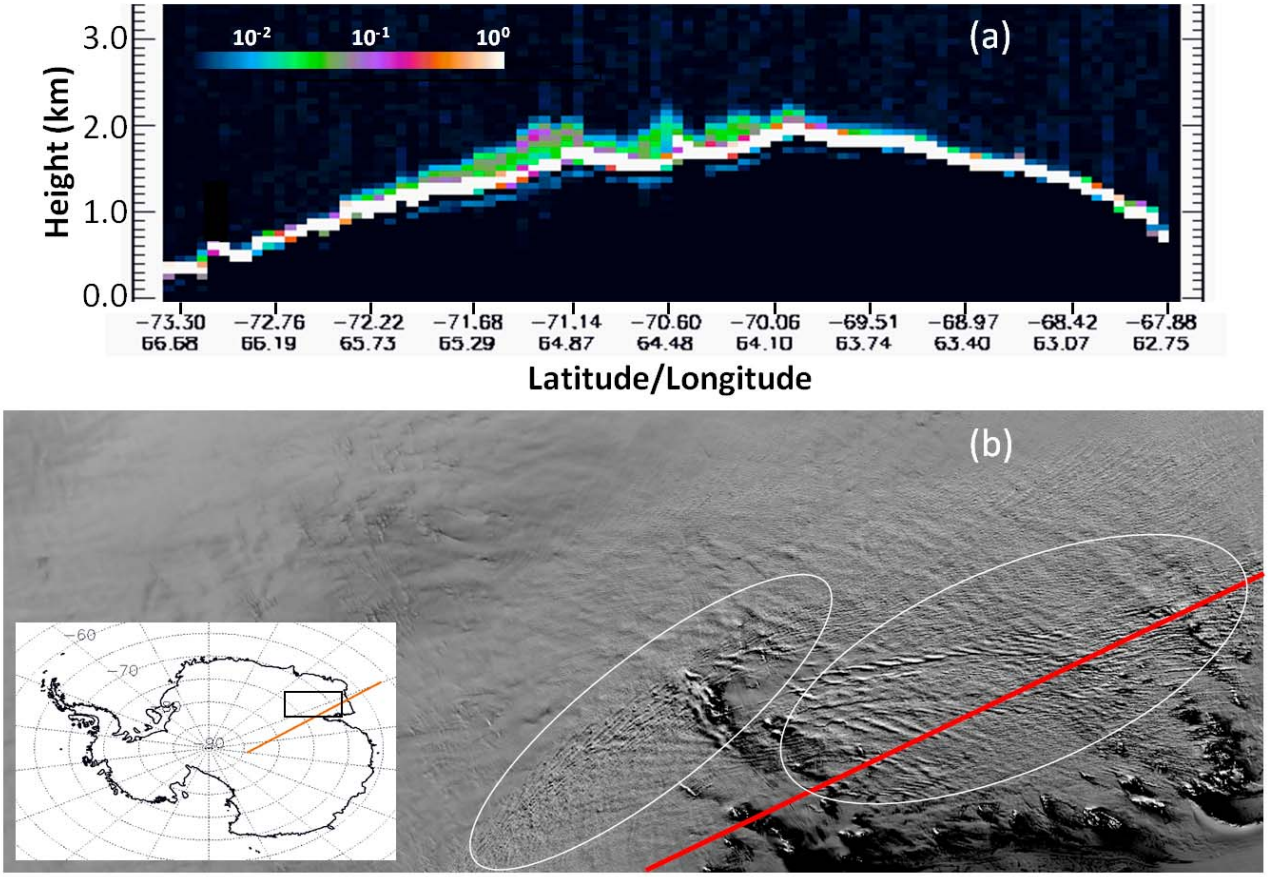

Figure 2. Blowing snow layer detected by ICESat on 22 February 2004 at 12:08 UTC over Antarctica. (a) The 532 nm attenuated backscatter for a portion of the track in inset (red line) in Figure 2b. (b) MODIS visible image at 10:00 UTC, 22 February 2004 covering the area within the square box on the inset. The white ovals demarcate the regions of blowing snow as evidenced by "billows" or "streets" seen in the image. The red line drawn on the MODIS image is the approximate position and extent of the ICESat ground track for the data shown in Figure 2a.

CALIPSO has an advantage in that it is part of the PM orbit constellation of Earth satellites and collocated data from other instruments are readily available (MODIS, Clouds and the Earth's Radiant Energy System (CERES), etc.). However, many blowing snow events were detected from the ICESat data. Examples are presented below.

[11] ICESat was launched in January 2003 and obtained data in 33 day long operation periods 3 times per year from 2003 until 2009. In addition to the altimetry channel, ICESat had two atmospheric channels at 532 and 1064 nm. Figure 2 shows a blowing snow case captured by ICESat on 22 February 2004 (12:08 UTC) in the area about 100 km inland from the Amery ice shelf. Figure 2a is an image of attenuated backscatter along the portion of the ICESat track that includes the blowing snow layer that is located roughly between latitudes 72.2°N and 69.0°N. The white pixels in the image represent the ground return, and the other colors are from atmospheric scattering (the blowing snow layer). The magnitude of the backscatter is shown on the color bar in the upper left and is generally between 5.0×10^{-2} and 1.0×10^{-1} km^{-1} sr^{-1}. Note that the scattering cross section of the blowing snow is similar in magnitude to what is measured by CALIPSO in Figure 1. The blowing snow layer varies in thickness between about 100 and 400 m. Note that what appears to be undulations of the layer top are also present. Figure 2b is a visible MODIS image taken of this area 2 h prior to the ICESat pass. The red line marks the approximate position of the ICESat track, which is also shown on the map to the left. On that map, the rectangular box encompasses the approximate area covered by the MODIS image. In the image, the areas within the white ovals show an alignment of billows consistent with the blowing snow as observed over Terra Nova Bay, Antarctica by *Scarchilli et al.* [2010]. We compared this MODIS image with another (not shown) of the same region and similar Sun elevation angle on a day when no blowing snow was detected by ICESat and none of these billow-type features were observed. In that image, the area within the white ovals looked smooth and featureless, very much like the region on the left half of the MODIS image shown in Figure 2b. We also know that these are not ground features because ICESat is able to fly nearly exact (within 100 m or less) repeat ground tracks. We compared the ICESat data in Figure 2a with repeat track data from a totally clear day (no blowing snow) from October 2003, and all that was seen was the ground return in the exact position as in Figure 2a.

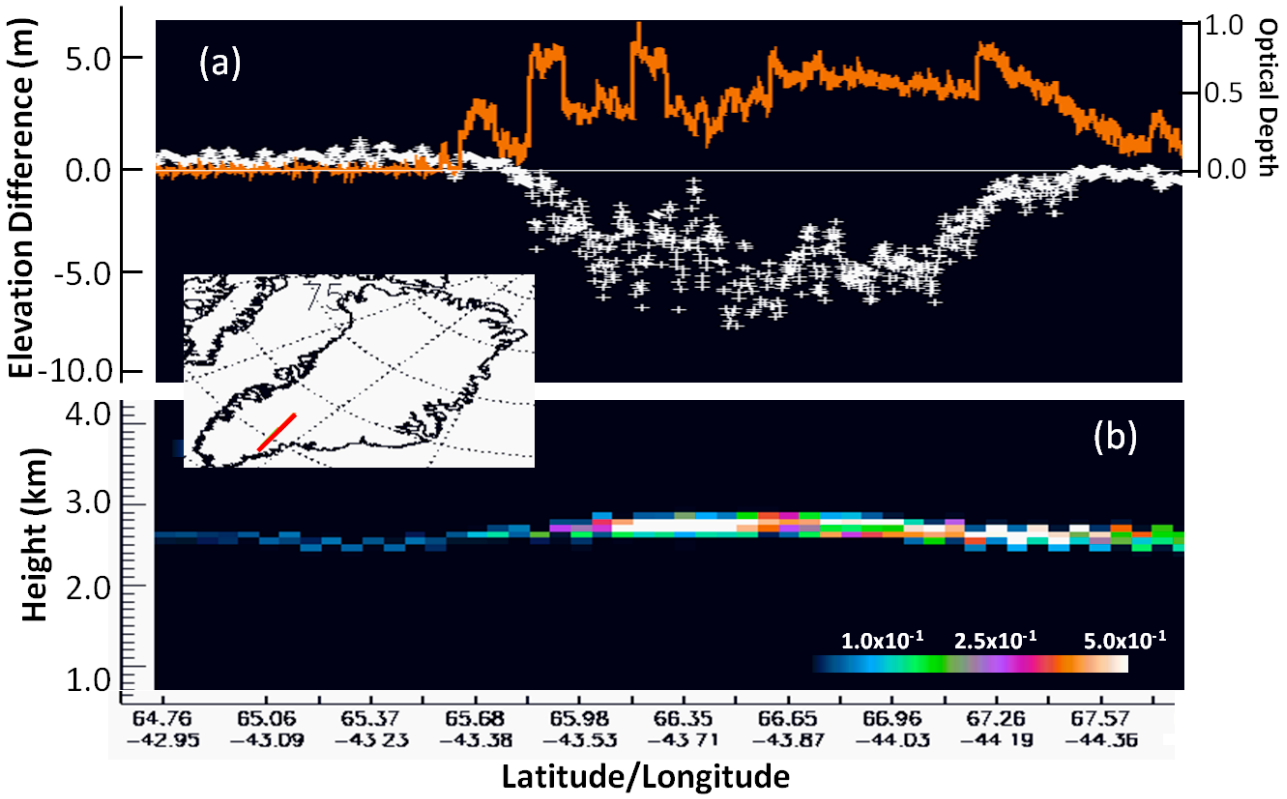

Figure 3. Blowing snow layer detected by ICESat over southern Greenland on 23 October 2003. (a) The difference in ICESat measured elevations between 23 October 2003 and 11 October 2004 along the same track (white pluses). (b) The 532 nm attenuated backscatter along the segment shown on the map (red line on map). Also shown in Figure 3a is the optical depth of the blowing snow layer (orange line and axis on right).

[12] Many such areas of blowing snow were detected by ICESat over Antarctica and also over Greenland. A major defining goal of the ICESat mission was precision altimetry and height change detection of the polar ice sheets. The stated goals were a single-pulse accuracy of 10 cm and temporally averaged change detection to 1.5 cm accuracy. Since ranging errors caused by pulse spreading are typically larger for layers close to the surface, detecting the presence of blowing snow is especially important. Although a full treatment of these effects is beyond the scope of this paper, we present here an example of the impact that blowing snow can have on the surface elevation retrieval of ICESat. Figure 3b shows the 532 nm attenuated backscatter as a function of altitude (above sea level) for a short segment over southern Greenland (red line on map) for which the ICESat algorithm detected blowing snow (23 October 2003, 21:51 UTC). Initially, the atmosphere is clear with no atmospheric scattering south of latitude 65.68°N. North of that, however, there are one to three ICESat bins (equivalent to 75–225 m) above the ground return that exhibit a very large backscattering magnitude. The main region of blowing snow is between latitudes 65.8°N and 67.4°N. The blowing snow is evidenced by the backscatter magnitude itself and the effect it has on the elevation retrieval shown in Figure 3a. Figure 3a displays the difference between elevation retrievals from 23 October 2003 and 11 October 2004 along this ground track. On the first day (23 October 2003), there was a blowing snow layer present, but it was totally clear on the second day (11 October 2004). The white plus signs shown in Figure 3a are the surface elevation retrieval on 23 October 2003 minus the surface elevation as determined from the 11 October 2004 data. Remember that ICESat is sampling along the same ground track (within 100 m) and the difference seen cannot be attributed to a change in the surface. Also shown in Figure 3a is the optical depth of the layer estimated from the ICESat atmospheric data (red line and axis on right). One can see a distinct correspondence between the elevation difference and the onset and waning of the blowing snow layer (i.e., between 65.7°N and 67.4°N). Multiple scattering of some photons within the blowing snow layer produces a range delay of the laser pulse centroid, thereby making the elevation appear lower. Thus, when the elevation determined from a clear day is subtracted from the elevation determined with blowing snow present, the result is negative as seen in Figure 3a. This effect depends on the optical depth of the blowing snow layer, its geometric thickness, and the characteristics of the blowing snow particles themselves.

4. Synergy of MODIS and CALIPSO

[13] The MODIS instrument aboard the AQUA satellite flies in formation with CALIPSO as part of the PM orbit (equator crossing at 13:30 LT) or so-called A-train constellation of Earth remote sensing satellites [see *Stephens*

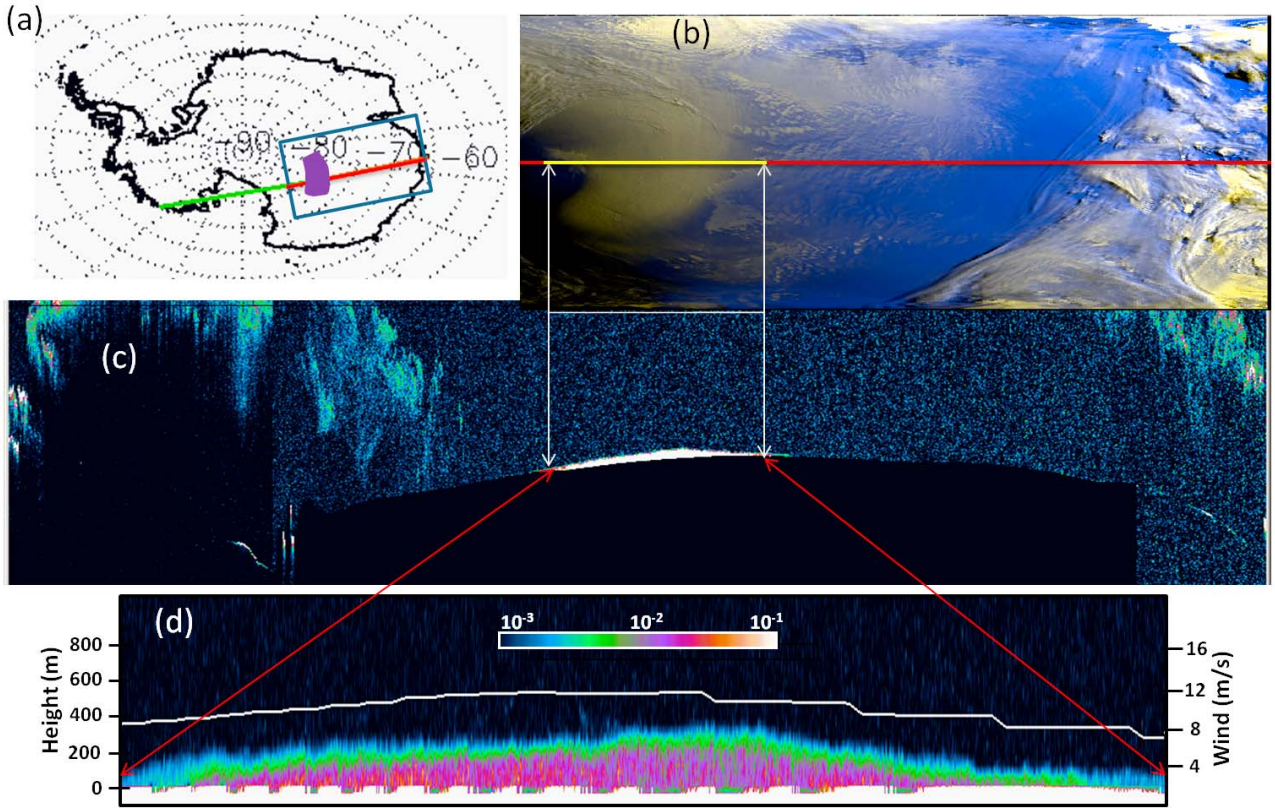

Figure 4. Blowing snow detected by CALIPSO and MODIS on 13 October 2009, 08:46 UTC, over East Antarctica. (a) Map of the CALIPSO/MODIS flight track with box indicating the area covered by the MODIS image shown in Figure 4b. (b) The CALIPSO track (red/yellow line) and a false color MODIS image (see text for description) showing the blowing snow region (grayish area between arrows). (c) The blowing snow detected by the algorithm shown as the white area between the arrows and (d) magnification of white area in Figure 4c. The color bar in Figure 4d shows the range of backscatter magnitude (km^{-1} sr^{-1}) within the blowing snow layer.

et al., 2002]. MODIS is a 36-channel scanning radiometer and obtains spatially and temporally coincident data with respect to CALIPSO (it is about 70 s ahead of CALIPSO in the A-train orbit). We can thus use MODIS data to help validate the CALIPSO retrievals of blowing snow. However, blowing snow detection from passive satellite instruments such as MODIS is difficult. In the visible, there is usually little contrast between the blowing snow and the underlying surface, since the latter is likely snow- or ice-covered (unless the blowing snow organizes into the long linear features discussed in section 3 and the Sun angle is optimal). In the long-wavelength channels, there is little thermal contrast between the suspended snow particles and the cold surface. In the shorter IR channels (3–4 μm), the blowing snow and snow surface both emit and reflect radiation similarly, making the blowing snow layer indistinguishable from the snow or ice surface both day and night. However, in the 1.6–2.1 μm region, clouds and suspended particles generally reflect more incoming solar radiation than features on the ground including snow and ice because the particles are smaller. This wavelength range thus offers the best chance at routinely detecting blowing snow, but since most of the radiation is reflected solar, this method is limited to sunlit scenes.

[14] For cases where the Sun was above the horizon, results of the blowing snow detection algorithm can be compared with simultaneous observations from MODIS. We have found that construction of a false color image using the 2.1 μm channels as red and green and the 0.85 μm visible channel as blue produces an image where the blowing snow layer stands out from the underlying white surface most prominently. An example of this is shown in Figure 4b, which displays the MODIS data along the CALIPSO segment shown in Figure 1 (13 October 2009). The CALIPSO track is overlain on the MODIS data in red and the portion of the track where blowing snow was detected is colored yellow. Notice the position of the yellow line with respect to the underlying MODIS data that in this area are a slightly grayish yellow that stands out from the underlying ice/snow surface that shows up mainly as blue. This is the blowing snow area. Notice that its left and right boundaries correspond well to the beginning and end of the CALIPSO blowing snow detections. The CALIPSO track is plotted on the map in Figure 4a as is the area covered by the MODIS data (blue box on map). Also shown on the map are the approximate shape and area of the blowing snow region as identified in the MODIS image (purple polygon within the box). The size of the blowing snow region is enormous, covering an area roughly 1000 by

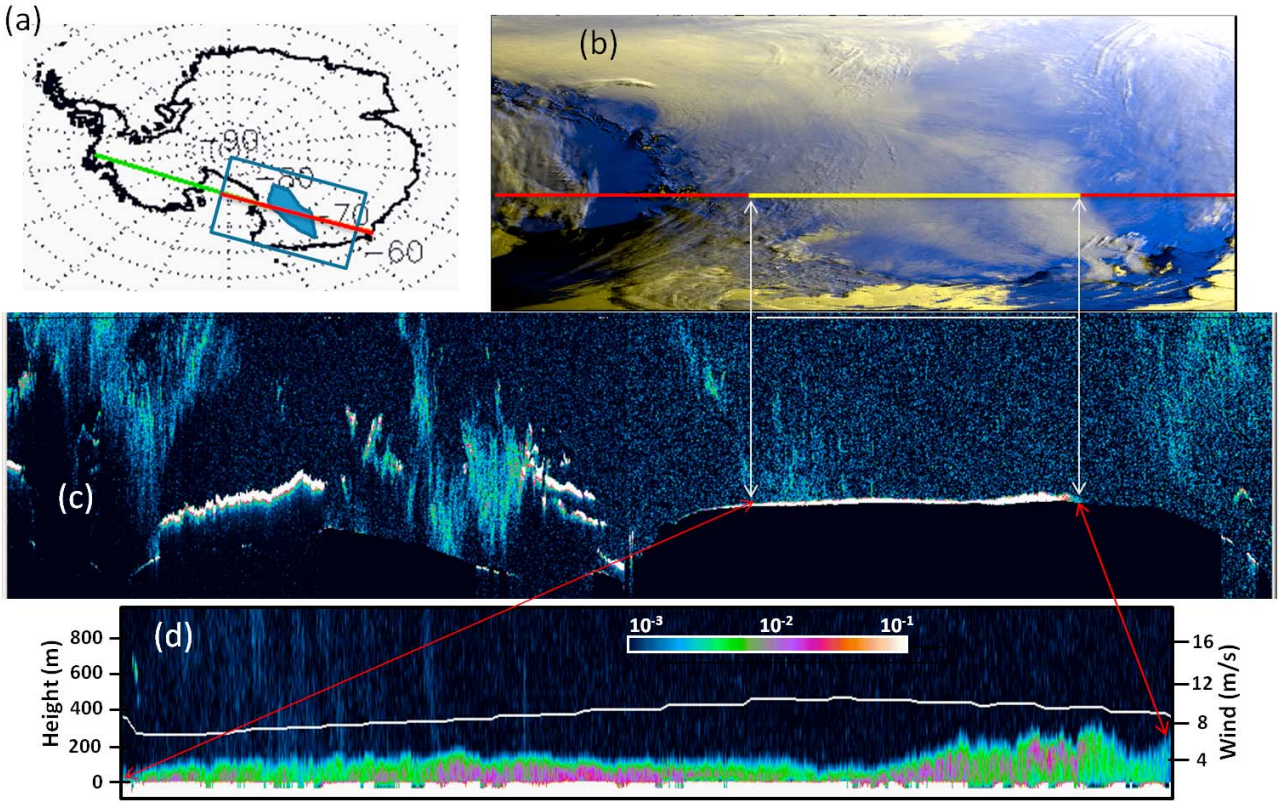

Figure 5. Same as Figure 4 except for 14 October 2009 at 06:13 UTC.

500 km (the length of the detected blowing snow along the CALIPSO track is 550 km). In addition, we are confident that the layer we are seeing in the CALIPSO data and have identified as blowing snow is, in fact, a part of a long-lived blowing snow "storm" throughout this region that lasted 3 days. In addition to the MODIS data, further evidence for this conclusion is provided in Figures 5 and 6. Figure 5 is the same as Figure 4 except for the following day (14 October 2009). The blowing snow region is larger than what was seen on 13 October, but is in the same general region of Antarctica. Figure 6 shows all of the CALIPSO blowing snow detections (in this region) for the period 13–15 October 2009. The solid colored lines are the detections for 13 October. The dashed lines are the CALIPSO blowing snow detections for 14 October, and the black lines are the detections for 15 October. On 12 or 16 October, there was very little blowing snow detected in this region. Thus, this event, which lasted 3 days, can be considered a blowing snow "storm" that formed quickly and transported a large quantity of snow a considerable distance from the continent to the Ross Sea. This is discussed further in section 6, but first we present a short discussion on the validation of the blowing snow retrievals.

5. Validation

[15] While MODIS can be used to bolster confidence that a detected layer is blowing snow, it cannot be used to verify that what is being retrieved from the lidar data is indeed blowing snow. True validation requires simultaneous ground observations for a close-by satellite overpass. Obviously, in Antarctica, this is difficult to obtain because of the scarcity of surface observations, especially in areas where blowing snow is most frequent. However, we were able to find a few close satellite passes to the Russian Vostok scientific station (78.867°S, 106.833°E) during conditions that were reported as "heavy blowing snow" from the ground observations there (see Table 1). Figure 7 shows the position of three CALIPSO ground tracks in relation to Vostok station (plus on the map) for 13 October 2009 and 9 April 2009. The ground tracks shown are only those portions for which blowing snow was detected. Also displayed in Figure 7 is the CALIPSO-measured attenuated backscatter along the plotted ground tracks with the 10 m wind speed plotted on the images (white lines, axis on right). Table 1 lists the near-simultaneous ground observations that were recorded at Vostok station for synoptic times before and after the CALIPSO observations. Note the reports of "heavy blowing snow" with zero visibility. These observations are within 2 h of the three CALIPSO overpasses. On 13 October, the CALIPSO passes were roughly 50–100 km from Vostok, but on 9 April 2009, CALIPSO passed within 5 km of Vostok. It is apparent that what we are interpreting as blowing snow in the CALIPSO data is indeed blowing snow, since it was nearly simultaneously observed by the ground observations at Vostok.

[16] While not validation per se, it is informative to examine the surface winds in relation to the blowing snow retrievals. In Figures 8a and 9a we show all of the blowing snow detections for 5 and 7 October 2009, respectively. In Figures 8b and 9b, the 12:00 UTC Antarctic Mesoscale

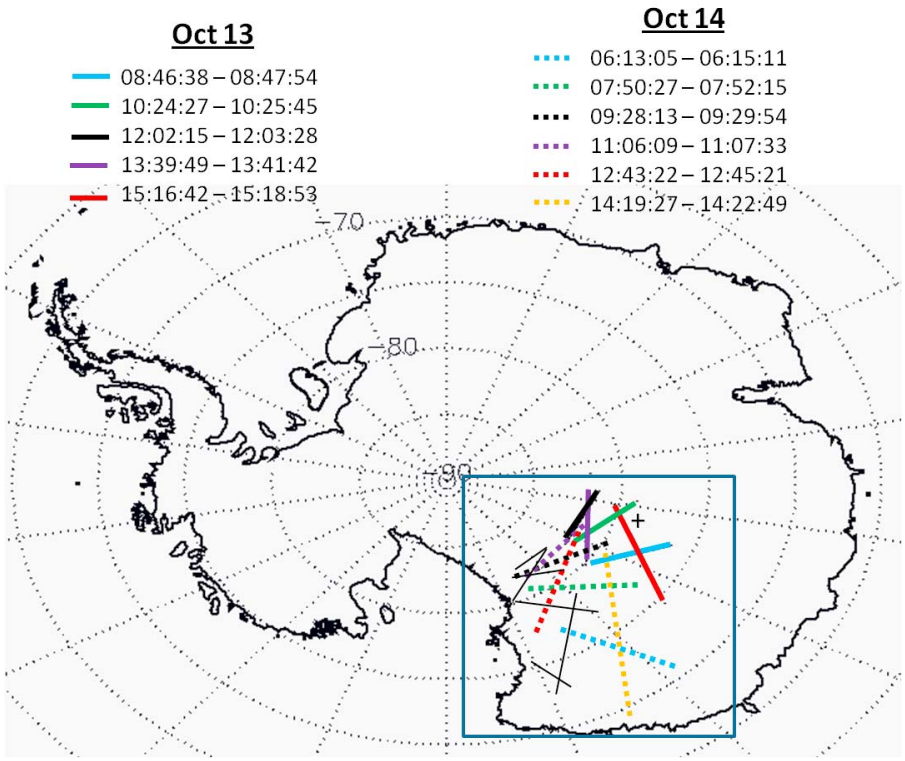

Figure 6. The spatial distribution of blowing snow detections from CALIPSO in the region bounded by the blue box for the period 13 October through 15 October 2009. For 13 and 14 October, the times of the blowing snow detections are shown at the top. The 15 October 15 detections are indicated by the solid black lines.

Prediction System (AMPS) 10 m wind speed for these days is shown, as are the detected areas of blowing snow (ovals). The AMPS is a mesoscale model used for real-time prediction of Antarctic weather and employs the Polar MM5, a version of the fifth-generation Pennsylvania State University–NCAR Mesoscale Model optimized for use over ice sheets [*Bromwich et al.*, 2005; *Monaghan et al.*, 2005]. It can be seen that each of the detected blowing snow regions corresponds to areas of high wind speed. The areas where blowing snow is occurring are associated with winds averaging 12–14 m s^{-1}. Note, however, that there could be other regions of blowing snow occurring on these days that are obscured by overlying particulate layers and thus undetectable by CALIPSO. This occurs most often in coastal regions and in West Antarctica. Also, note the area of blowing snow centered at about 150°E and 76°S in Figure 9. This is an enormous area, larger in size than the state of Alaska, and is another demonstration of the size of blowing snow storms that may often occur over Antarctica. It is likely that this blowing snow region is being transported by high winds from the continent to adjacent sea ice and ocean areas. We examine such mass transport events in more detail in section 6.

6. Mass Transport

[17] It has been suggested by others that the transport and sublimation of blowing snow can lead to significant mass loss during strong winds and can be an important factor in the surface mass balance of the Antarctic ice sheets [*Pomeroy and Essery*, 1999; *Bintanja*, 2000; *Déry and Yau*, 2002; J. Lenaerts and M. van den Broeke, Regional climate modeling of snowdrift in Antarctica: 2. Results, submitted to *Journal of Geophysical Research*, 2011]. Here we estimate the horizontal blowing snow mass transport associated the blowing snow event on 13–15 October 2009. While the lidar data cannot be used to directly measure the mass of the blowing snow layer, the data can be used for a first-order

Table 1. Surface Observations at Vostok Station, Antarctica, Closest in Time to the Blowing Snow Retrievals Shown in Figure 7

Date/Time (UTC)	*T*(°C)	RH(%)	Wind Speed (m s^{-1})	Wind Direction	Visibility (km)	Surface Conditions
9 April 2009/12:00	−63	36	7.2	SSW	1.6	blowing snow
9 April 2009/18:00	−63	36	7.2	S	0	blowing snow
13 October 2009/06:00	−53	38	10.3	WSW	0	heavy blowing snow
13 October 2009/12:00	−53	38	11.4	SW	0	heavy blowing snow
13 October 2009/18:00	−56	29	10.3	SW	0	heavy blowing snow

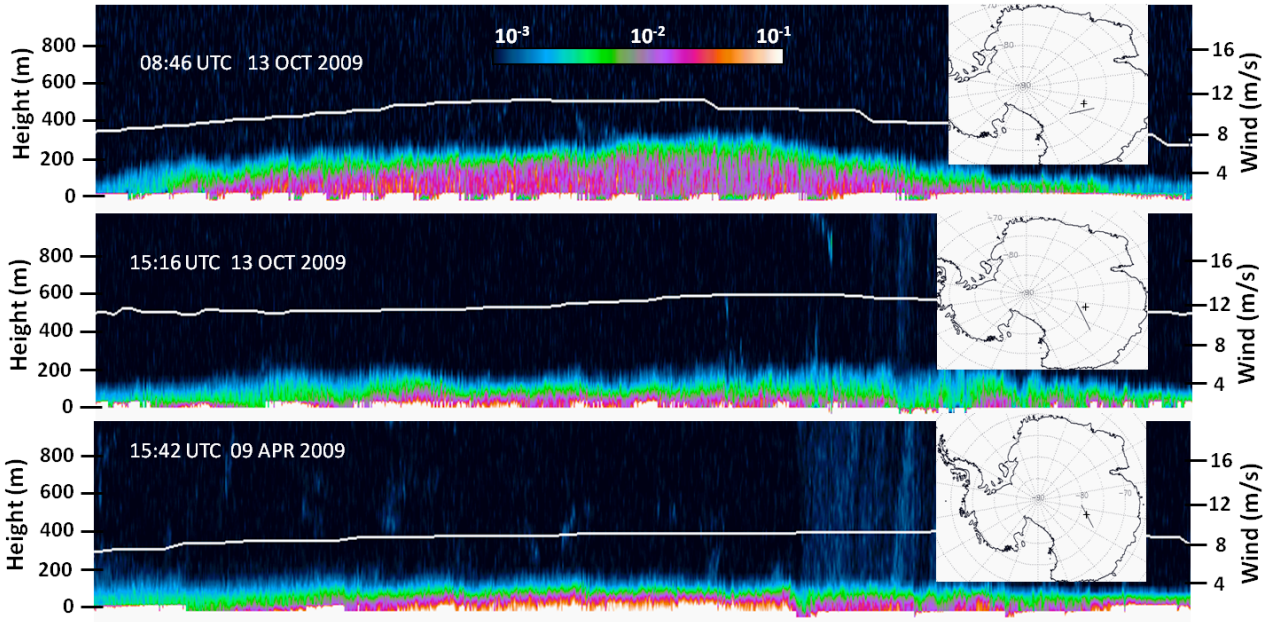

Figure 7. CALIPSO 532 nm backscatter for three relatively close passes (lines on map) to Vostok Station (plus sign on the map) on 9 April 2009 and 13 October 2009. The wind speed from the CALIPSO data product is plotted on the backscatter images (white line, axis on right) as is the time in UTC. See Table 1 for surface conditions at Vostok near the times of the satellite overpasses.

estimate of the mass based on the scattering magnitude within the layer. Backscattering of light by a snow particle is proportional to its projected area, and the volume attenuation (or extinction) cross section in blowing snow is a function of the square of the particle size and the number of particles per unit volume [*Schmidt*, 1982]. The volume extinction cross section (σ), which can be estimated by lidar, may be assumed related to the number density of scattering particles (N) as

$$N = \sigma / 2\pi r^2 \tag{1}$$

where r is the average radius of the suspended snow particles. While many field campaigns have provided measure-

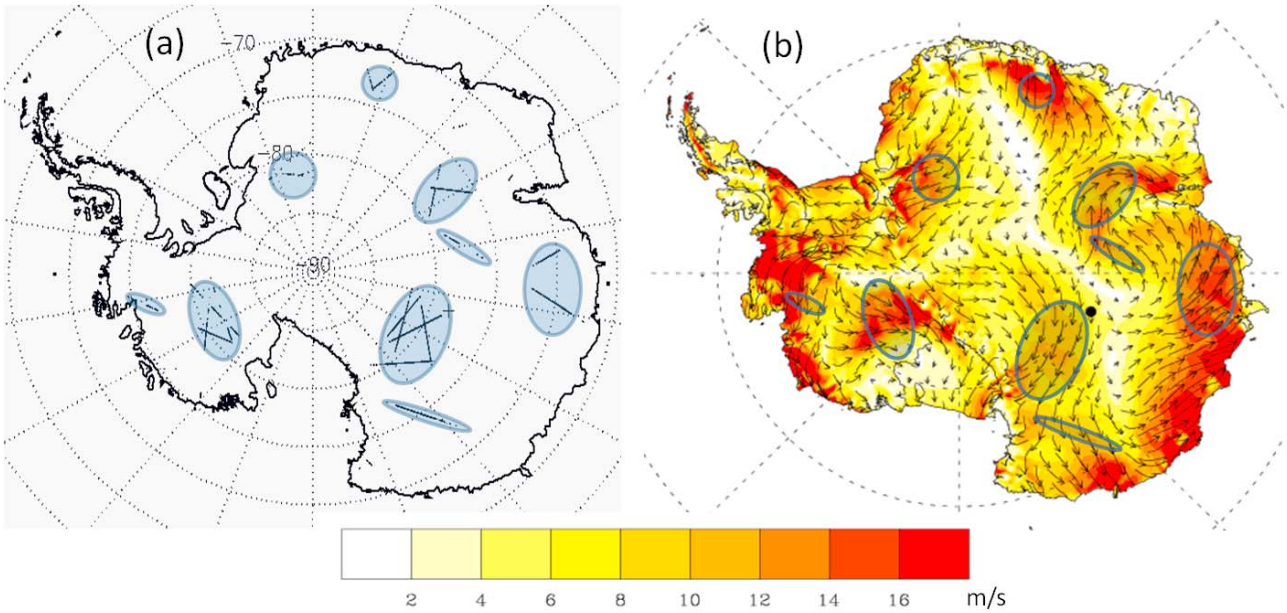

Figure 8. (a) All CALIPSO blowing snow detections for 5 October 2009 and (b) the AMPS 10 m wind velocity for 12:00 UTC on 5 October 2009. In both Figures 8a and 8b, the areas of blowing snow are indicated by the ovals.

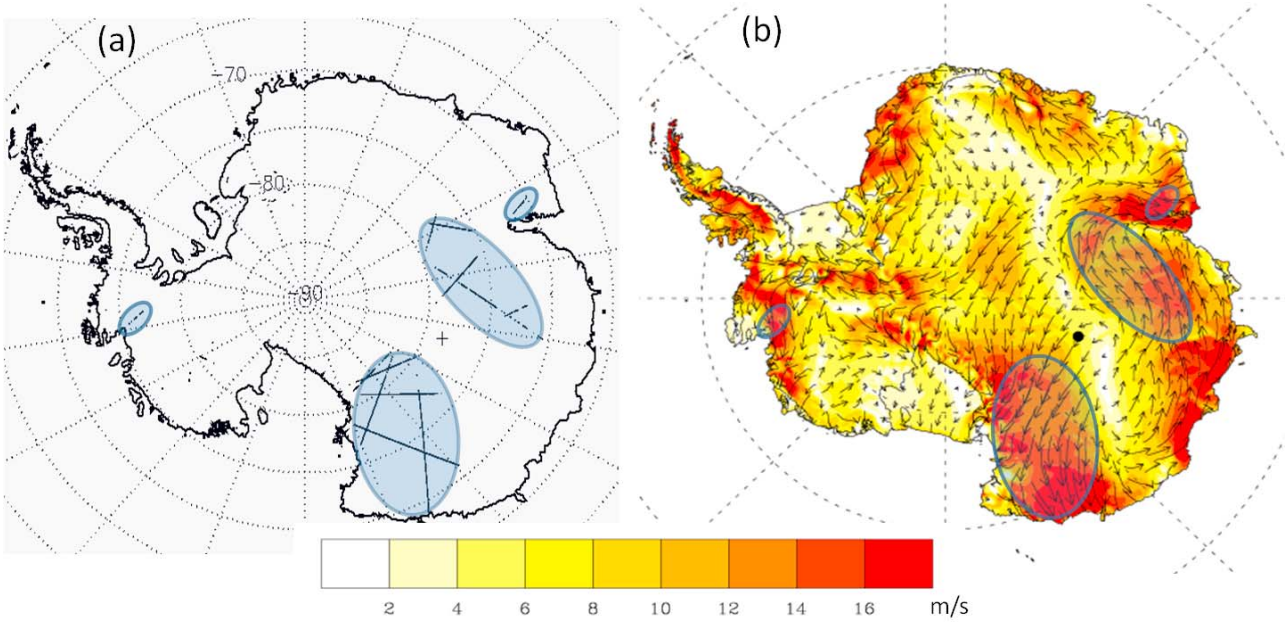

Figure 9. Same as Figure 8 except for 7 October 2009, 12:00 UTC.

ments of blowing snow particle size [*Mann et al.*, 2000; *Nishimura and Nemoto*, 2005; *Walden et al.* 2003; *Lawson et al.*, 2006; *Gordon and Taylor*, 2009], they were generally made within the first few meters of the surface and may not be applicable to blowing snow layers as deep as those studied here. Most observations have shown a height dependence of particle size ranging from 100 to 200 μm in the lower tens of centimeters above the surface to 50–60 μm near 10 m height [*Nishimura and Nemoto*, 2005]. A notable exception is the result of *Harder et al.* [1996] at the South Pole, who measured the size of blowing snow particles during a blizzard by collecting them on a microscope slide. They report an average effective radius of 15 μm, but the height at which the measurements were made is not reported. From surface observations made at the South Pole, *Walden et al.* [2003] and *Lawson et al.* [2006] report an average effective radius for blowing snow particles of 11 and 17 μm, respectively. Given the discrepancy of the available observations and the fact that we know of no blowing snow particle size measurements above 10 m, we choose to use a snow particle of spherically equivalent radius of 30 μm, which is intermediate between the available observations. It should be further noted here that using an assumed particle size of 30 μm and an average extinction of 2.0 km^{-1} in equation (1) yields a particle number density of 3.5 × 10^5 m^{-3}, which is in the middle of the range measured by *Mann et al.* [2000] at the 10 m height.

[18] The mass per unit volume (M) is related to N through

$$M = 4/3\pi r^3 N\rho \tag{2}$$

where ρ is the density of ice. Substituting (1) into (2), we have the following:

$$M = 2r\rho\sigma/3 \tag{3}$$

The extinction (σ) can be estimated from the average backscatter cross section (β) that is directly measured by the lidar if the extinction to backscatter ratio (S) for the scattering layer is known. In practice, S varies significantly (10–120 sr) with particle size, shape, and composition. However, if something is known about the scattering particle, then the uncertainty of S can be narrowed considerably. For instance, the S value for cirrus clouds has a range of about 15–25 sr. For water clouds it is typically between 10 and 20 sr [*Yorks et al.*, 2011; *Whiteman et al.*, 2004]. Since direct measurements of S for blowing snow layers are not available, we will use an estimate of 20 sr to convert the measured backscatter to an estimate of the extinction. We consider this conversion to be accurate to within about 50%. Equation (3) now becomes

$$M = 2r\rho\beta S/3 \tag{4}$$

and then the total mass of the blowing snow layer is

$$M_{\mathrm{tot}} = 2r\rho\beta S V_{\mathrm{bs}}/3 \tag{5}$$

where V_{bs} is the total volume of the blowing snow "storm" and β is the average backscatter cross section of the blowing snow layer. The average area covered by the storm (an average of the 3 days shown in Figure 6) is roughly 500,000 km^2. The average depth of the layer (obtained by taking the average of the height of all blowing snow detections shown in Figure 6) is about 100 m (105.5 m). Thus, V_{bs}, the volume of the blowing snow layer, is about 50,000 km^3. The average backscatter cross section (β) for the lowest 100 m was determined to be 0.10 km^{-1} sr^{-1} (see Figure 13a). Inserting these values into equation (5) and using a value of 30 μm for the average effective snow particle size (r) and ice density of 916.7 kg m^{-3}, we obtain an estimate for the total mass of the blowing snow layer of

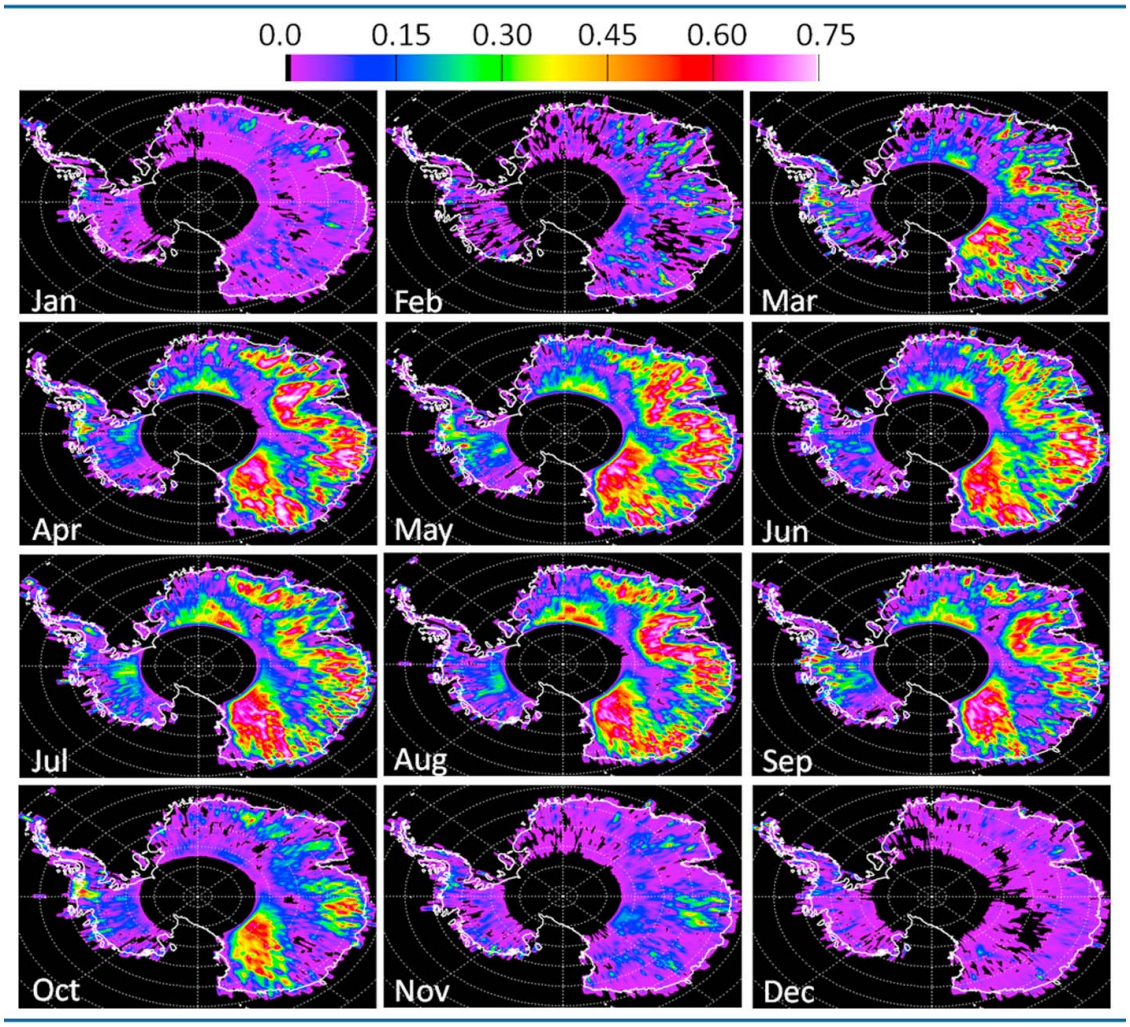

Figure 10. The blowing snow frequency (fraction) and spatial distribution over Antarctica for each month of 2009 as determined from analysis of CALIPSO data.

1.83×10^9 kg. While some of this mass is apparently transported long distances, some of the snow mass no doubt sublimates as it is kept aloft, moistening and cooling the atmosphere. However, modeling studies have shown that sublimation is a self-limiting process, decreasing as the relative humidity of the blowing snow layer increases [*Xiao et al.*, 2000; *Lenaerts et al.*, 2010]. So it is likely, in long-lived blowing snow events, that the blowing snow layer becomes saturated or nearly so, limiting the amount of sublimation. This would imply that most of the snow mass in this case is being transported from the continental interior to the surrounding sea ice and possibly the ocean. If the average wind speed through the depth of the blowing snow layer was 20 m s^{-1} (it was 12 m s^{-1} at 10 m height based on the AMPS model), then the horizontal mass transport rate of this event is $F = 1.83 \times 10^9$ kg $\times$ 0.020 km s^{-1}/50,000 km^3 = 733 kg km^{-2} s^{-1} = 7.3×10^{-4} kg m^{-2} s^{-1}, which equates to 63.3 kg m^{-2} d^{-1}. If we consider the whole 100 m blowing snow column, this is 7.3×10^{-2} kg m^{-1} s^{-1} or 6.3×10^3 kg m^{-1} d^{-1}. For comparison, *Mann et al.* [2000] report blowing snow fluxes integrated over the lower 12 m in the vertical of roughly 2×10^4 kg m^{-1} d^{-1}, and *Scarchilli et al.* [2010] report about 6.8×10^3 kg m^{-1} d^{-1}. *Schmidt* [1982] shows data from Mizuho Camp, East Antarctica, with transport rates ranging from about 8.0×10^2 to 10^4 kg m^{-1} d^{-1} for wind speeds ranging from 7 to 13 m s^{-1}. *Lenaerts et al.* [2010] report on three blowing snow events that occurred during the ENABLE campaign in January and February 2002, the strongest of which yielded a horizontal snow transport rate of 7.0×10^{-2} kg m^{-1} s^{-1}.

7. Blowing Snow Properties

7.1. Spatial and Temporal Frequency

[19] The near-surface wind speed and the state of the snow at the surface (age, density, and cohesive properties) determine the likelihood that snow particles will be lifted up and carried by the wind [*Li and Pomeroy*, 1997]. Thus, the spatial and temporal distribution of the frequency of blowing snow over Antarctica is expected to be influenced by the pattern of the katabatic winds that are maximum in the winter months and generally directed from the interior toward the coast. The results of modeling efforts have shown that blowing snow frequency generally follows the katabatic wind pattern over Antarctica with most of the blowing snow occurring in a band roughly 500 km wide that parallels the East Antarctic coast

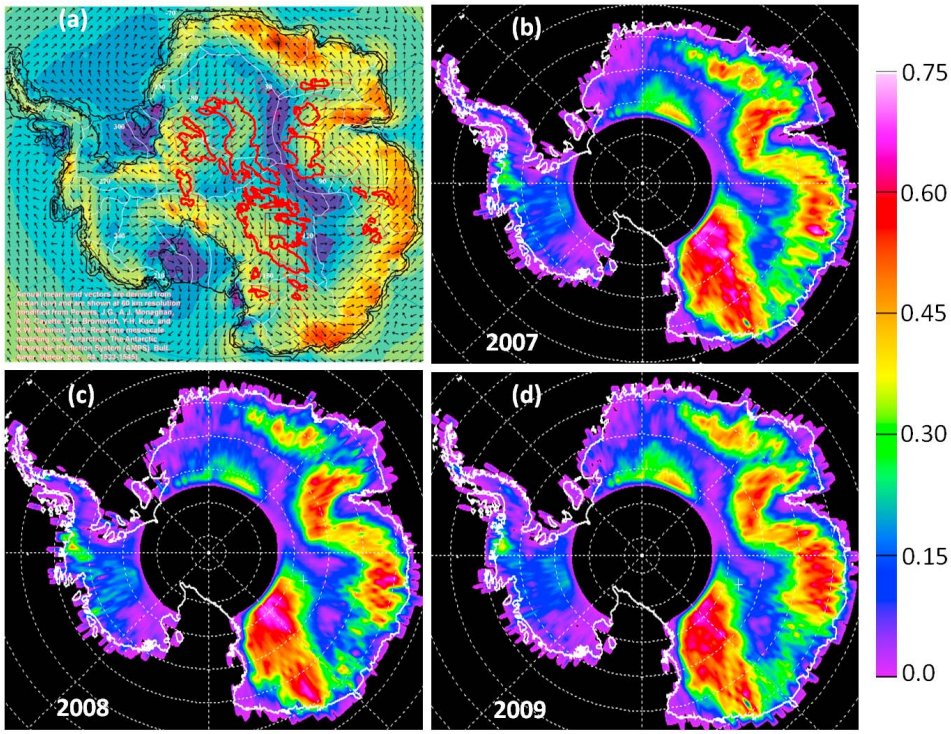

Figure 11. Annual mean wind vectors over and around Antarctica from (a) *Powers et al.* [2003] and the average (April through October) blowing snow frequency (fraction) for (b) 2007, (c) 2008, and (d) 2009 as derived from CALIPSO data. The color bar pertains only to the blowing snow frequency maps.

[*van de Berg et al.*, 2006; *van den Broeke et al.*, 2006; *Lenaerts et al.*, 2010].

[20] Only a small number of ground-based observations have been made in Antarctica that can give indications as to the frequency of blowing snow. Some supply year-round or multiyear statistics [*Mahesh et al.*, 2003], while others have data only for a few months of the year. *Mann et al.* [2000] present observations made at Halley Station (75.6°S, 26.7°W) throughout the 1991 austral winter. They find that blowing snow occurs between 27% and 37% of the time during winter (June, July, and August). *Mahesh et al.* [2003] examined surface observations over a number of years at the South Pole and determined that blowing snow was present 40% to 50% of the time during winter. In this section, we present the application of the blowing snow detection algorithm to three full years (2007, 2008, and 2009) of CALIPSO data over Antarctica. As noted in section 2, the blowing snow detections are limited to layers at least 20 m deep and for when overlying thick particulate layers do not attenuate the laser beam (layers of optical depth >1.5). Shallow blowing snow layers cannot reliably be detected and thus are not included in the data presented here.

[21] Figure 10 shows the monthly averaged composite of blowing snow frequency for each month of 2009 over Antarctica based on CALIPSO measurements. The monthly averages are generated by setting up a rectangular grid (1° × 1°) over Antarctica and counting the number of blowing snow detections within the grid box and dividing it by the total number of observations for that grid box. The observation count (denominator) is incremented only if the ground return is detected. Thus, if overlying particulate layers are present that are thick enough to prohibit the detection of the ground return, it does not count as an observation. This approach will help to keep areas that are often cloudy (parts of West Antarctica and coastal areas) from having blowing snow frequencies that are erroneously low. Figure 10 shows the strong seasonal dependence of blowing snow and that blowing snow is prevalent in all months except December and January. Note how quickly blowing snow frequency picks up as soon as the Sun sets (March) and autumn begins and remains high through late spring (October). In winter months and in certain areas, the frequency of blowing snow approaches and sometimes exceeds 70%.

[22] The average spatial distribution of blowing snow is very similar to the average strength of the katabatic wind distribution (Figure 11a) and prior modeling studies of blowing snow sublimation and transport (Lenaerts and van den Broeke, submitted manuscript, 2011), except for one notable difference. Figure 11 also shows the average blowing snow frequency over Antarctica for 2007, 2008, and 2009 for the months when blowing snow is most prevalent (April through October). For all years, the largest and most persistent maximum in the CALIPSO blowing snow frequency occurs in the megadune region of East Antarctica (from about 120°E to 160°E between latitudes 75°S and 85°S; The red lines in Figure 11a are outlines of megadune regions throughout Antarctica). This feature is not picked up in models of blowing snow frequency. The cause of the discrepancy is not clear and requires further study. We do not believe it to be a problem with the blowing snow retrieval or the CALIPSO data because many images (like Figures 4d and 5d) were made from the blowing snow retrievals in this

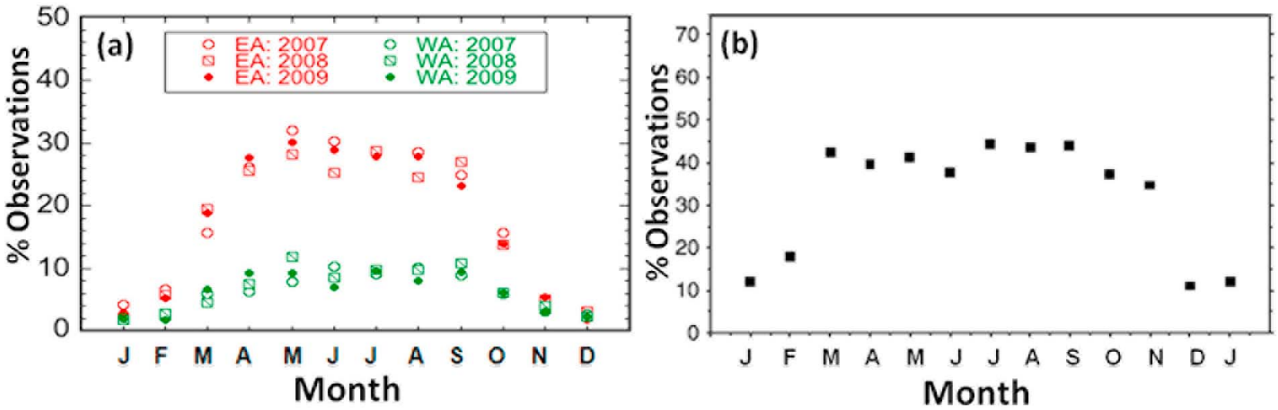

Figure 12. (a) Average blowing snow frequency by month for East (red) and West (green) Antarctica for 2007 (open circles), 2008 (open squares), and 2009 (solid diamonds) as derived from CALIPSO data. (b) Blowing snow frequency by month as determined from 12 years of ground observations at the South Pole [*Mahesh et al.*, 2003].

region as part of data quality efforts. No problems or "false-positive" retrievals were ever seen in the data. It should also be mentioned that blowing snow frequency obtained from ICESat data show the same pattern and it extends further south (to the limit of the observations (86°S)). Since the frequency of blowing snow depends on the physical characteristics of the snow on the surface and the surface wind speed, a reasonable conclusion is that, in the megadune region, the winds blow more consistently at high speeds and/or the availability of snow (with the proper physical characteristics that enable it to become airborne) is greater in this region. *Picciotto et al.* [1970] report that this area experiences very low snow accumulation rates (precipitation), and thus it seems unlikely that the latter reason is the cause of the high blowing snow frequency in this region. *Fahnestock et al.* [2000] also find unique firn conditions in the dune area with a preponderance of very coarse grained firn. Whatever the reason for the high blowing snow frequency in the megadune region, it is a very interesting and persistent feature that exists throughout the 3 years of CALIPSO data (and the ICESat data from 2003 and 2004) that have so far been analyzed.

[23] Figure 12a shows the monthly averaged blowing snow frequency for 2007, 2008, and 2009 for East (red) and West (green) Antarctica. There does not appear to be a trend in the data for either East or West Antarctica. However, year to year variability of the East Antarctic average blowing snow frequency can approach 20% for some winter months. It is likely that regional variability could be much larger. Also shown in Figure 12b are the *Mahesh et al.* [2003] data on the frequency of blowing snow at the South Pole. The orbit of CALIPSO is such that observations can be made only to 82°S, and thus a direct comparison with the South Pole statistics cannot be made. However, there are notable similarities in the two data sets with regard to seasonality. Also, the frequency of blowing snow is higher in all months at the South Pole, but this is at least partially because the Mahesh et al. observations include blowing snow layers that are fairly shallow and episodes that occurred with overlying cloud cover. In addition, the CALIPSO measurements shown in Figure 12a are an average over large regions. For instance, the very extensive blowing snow minimum over the high East Antarctic plateau is averaged into the data and will reduce the overall frequency considerably for the East Antarctic average.

7.2. Layer Backscatter Profile, Thickness, and Optical Depth

[24] Figure 13a shows the average backscatter coefficient profile for all blowing snow detections for the period April through October for 2007, 2008, and 2009 in the area of high blowing snow frequency that encompasses the megadune region (75°S–82°S, and 100°E–160°E). The average backscatter profile is almost identical for the 3 years (especially below 80 m), indicating that the average scattering characteristics of blowing snow layers in this region do not change very much from year to year. The backscatter magnitude ranges over a factor of about 50, and the profiles contain two inflection points at about 350 and 80 m, which are very interesting and probably related to the structure of the Antarctic boundary layer. Below 80 m the average backscatter increases sharply with values below 50 m exceeding 1.0×10^{-1} km^{-1} sr^{-1}. Figure 13b shows both the frequency distribution of blowing snow layer height (solid) and optical depth (dashed) detected in the megadune region for April through October 2009. There were a total of 1.6 million blowing snow observations within this region. The average layer thickness is 100 m, and the large majority of the blowing snow layers are 100 m or less in thickness (71%). Roughly 25% of the layers are between 100 and 300 m thick. Only 4% of the blowing snow layers are thicker than 300 m. Layers thicker than 500 m are very infrequent; they occur just 0.8% of the time. The average optical depth of the blowing snow layers is 0.1, but there is a wide variation between 0.05 and 1.0. Layers with optical depth greater than 0.8 are very rare (0.1%). No blowing snow layers in this region were detected with optical depth greater than 1.0. The optical depth is a measure of how much the laser radiation is attenuated (scattered or absorbed) as it travels through the layer. A value of 1.0 would be typical of fairly thick cirrus clouds, and 0.2 would be a common value for an aerosol-laden boundary layer roughly

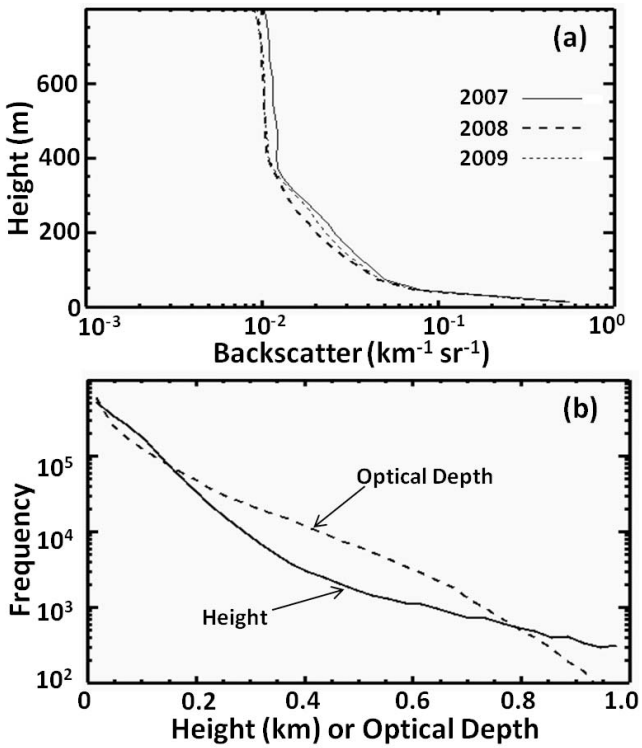

Figure 13. (a) The average (April through October) attenuated backscatter profile through all blowing snow layers detected over the megadune region for 2007, 2008, and 2009. (b) The frequency distribution of (solid line) blowing snow layer thickness and (dashed line) optical depth for April through October, 2009 for the same region.

1 km deep. As discussed in section 6, the optical depth is estimated from the layer average backscatter and geometrical depth using an assumed extinction to backscatter ratio of 20 sr. Using this method, we expect the optical depth measurements to be accurate to within about 50%.

[25] An interesting and significant relationship to examine is the frequency distribution of wind speeds when blowing snow is present (detected) compared with the distribution of wind speed when it was not detected. Figure 14 shows this for the same region and time as the optical depth and layer height discussed above (megadune region). We see that the highest frequency of blowing snow occurs at a wind speed of 9 m s^{-1} with very little blowing snow below a wind speed of 5–6 m s^{-1}. *Mahesh et al.* [2003] analyzed South Pole data from 1989 to 2001 and plotted the frequency distribution of (10 m) winds speeds as is done in Figure 14. Their result is very similar, but the maximum frequency of blowing snow occurs at a slightly lower average wind speed (7.5 m s^{-1}), and blowing snow is equally likely to occur as to not occur at a wind speed of 6 m s^{-1}. Also plotted in Figure 14 is the average optical depth (pluses) of the blowing snow layers as a function of wind speed. There is an almost linear increase in optical depth with wind speed between 4 and 7 m s^{-1}, and it increases most rapidly between 8 and 12 m s^{-1}. This behavior makes sense physically because higher wind speeds can be expected to loft more snow particles into the air and also possibly carry them higher into the atmosphere.

8. Summary and Conclusions

[26] In this paper we have presented a technique for the detection of blowing snow using satellite lidar data from ICESat and CALIPSO. We have shown, for the first time, the temporal and spatial frequency of blowing snow events over Antarctica for three complete years (2007 through 2009) based on satellite lidar retrievals. We find that the frequency of blowing snow approaches 70% over certain regions of East Antarctica during winter, and this is largely associated with the average katabatic wind pattern. A notable exception is found in the megadune region (120°E to 160°E, 75°S to 85°S) of East Antarctica which has the largest and most persistent area of blowing snow, but not necessarily the strongest winds, on average. A link between the megadunes and the high frequency of blowing snow was hypothesized, but at present the cause and effect are not clear. The spatial pattern and frequency of blowing snow do not change much from year to year, but during winter, interannual variability of up to 20% is noted for East

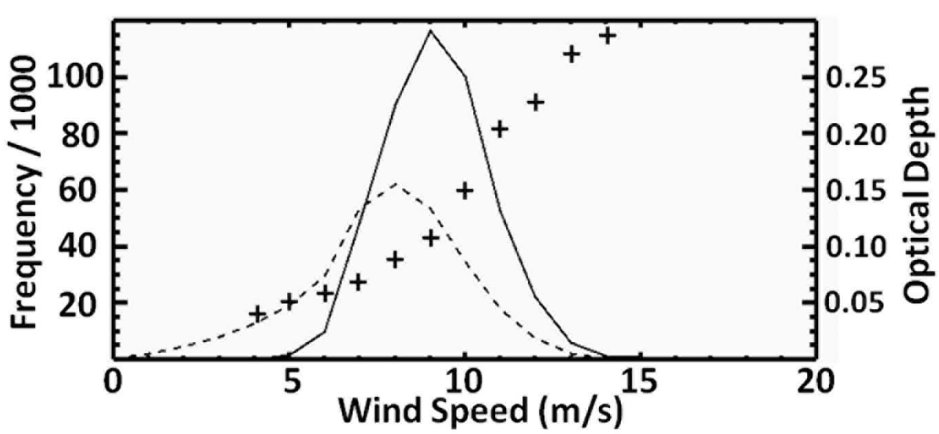

Figure 14. The frequency distribution of wind speed for all blowing snow detections (solid line) and all nonblowing snow observations (dashed line) for April through October 2009 for the megadune region. Also shown is the average blowing snow layer optical depth as a function of wind speed (pluses; axis on right).

Antarctica. However, there does not appear to be a region-wide trend to the average blowing snow frequency for the 3 year period examined here.

[27] The optical depth, thickness, and backscatter properties of blowing snow layers were determined from the lidar data. Average thickness of the blowing snow layers is 120 m, and the thickness varied between the minimum detectable height (30 m) and 1000 m. Only 0.8% of the layers was greater than 500 m in thickness. The average optical depth of blowing snow layers is 0.2, and it varied between about 0.05 and 1.0. A clear correlation between layer optical depth and surface wind speed was demonstrated for blowing snow over the megadune region of Antarctica.

[28] MODIS data, collocated in space and time with CALIPSO data, were used synergistically to identify two blowing snow regions. By constructing a false color image using the 0.85 and 2.1 μm MODIS channels, the blowing snow regions were easily visible in the image against the ice and snow background. However, this method is limited to sunlit scenes. Sometimes, as was noted in one of the two ICESat cases presented, the blowing snow becomes organized into long, linear, relatively thick (300–400 m) "billows" that are plainly apparent in visible satellite imagery. This has also been noted and discussed by other authors [*Scarchilli et al.*, 2010]. We demonstrated the large effect (up to 8 m caused by multiple scattering) that blowing snow layers can have on spaceborne altimetry via an examination of ICESat altimetry data over Greenland. Future planned NASA spaceborne laser altimetry instruments such as ICESat-II and DESDyni will also experience errors caused by multiple scattering within blowing snow, making it very important to better understand the properties and climatology of blowing snow over Antarctica and Greenland. This paper is the first step toward that goal.

[29] The mass balance of the Earth's two great ice sheets in Greenland and Antarctica is a topic of great interest and importance because it relates to global climate change and sea level rise. Although it has been intensively studied in recent years, it is still not very well understood, and blowing snow is known to play a major role through the transport and sublimation of snow. The possible mass transport by blowing snow is sometimes dismissed as not significant compared with glacial ice flow and ocean interface melting. However, we have shown the existence of large blowing snow "storms" over parts of East Antarctica that last for several days. We developed a technique to estimate the mass transport involved in one such storm that occurred over a 3 day period in October 2009. We found a mass transport value of 6.3×10^3 kg m^{-1} d^{-1} which is of comparable magnitude to field measurements of blowing snow transport. Further analysis leading to overall estimates of mass transport off the continent is possible. In addition to the effect on the ice sheets, the movement of snow onto sea ice and its impact on persistence of sea ice is of interest and an effect that should be analyzed.

[30] The observations presented here are unique and of value to both cryospheric and atmospheric processes. Further work will include an investigation of blowing snow over sea ice and a complete analysis of the CALISPO and ICESat data to obtain a longer historical record of blowing snow properties over both Antarctica and Greenland. In addition, the satellite lidar analysis could be used to test the use of other remote sensing instruments such as the Multiangle Imaging Spectroradiometer and advanced very high resolution radiometer (AVHRR) for blowing snow detection and characterization for extension to larger areas and time frames. Of importance to climate change is whether there is any trend to blowing snow frequency over Antarctica in recent years. Construction of a longer blowing snow frequency time series through use of these methods can help answer that question.

[31] **Acknowledgments.** The authors are sincerely grateful to Thomas Wagner, the Cryosphere Program Manager at NASA Headquarters, for providing the funding and encouragement to perform this blowing snow study. We also thank the NASA Langley Research Center's Atmospheric Science Data Center for supplying the CALIPSO data used in this research and Julien Nicolas of the Byrd Polar Research Center at Ohio State University for supplying the AMPS 10 m wind speeds.

References

Bintanja, R. (2000), The surface heat budget of Antarctic snow and blue ice: Interpretation of spatial and temporal variability, *J. Geophys. Res.*, *105*, 24,387–24,407.

Bromwich, D. H., A. J. Monaghan, K. W. Manning, and J. G. Powers (2005), Real-time forecasting for the Antarctic: An evaluation of the Antarctic Mesoscale Prediction System (AMPS), *Mon. Weather Rev.*, *133*, 579–603, doi:10.1175/MWR-2881.1.

Brümmer, B. (1999), Roll and cell convection in wintertime arctic cold-air outbreaks, *J. Atmos. Sci.*, *56*, 2613–2636, doi:10.1175/1520-0469(1999)056<2613:RACCIW>2.0.CO;2.

Budd, W. F., R. Dingle, and U. Radok (1966), The Byrd snow drift project: Outline and basic results, in *Studies in Antarctic Meteorology*, *Antarctic Res., Ser*, vol. 9, edited by M. Rubin, pp. 71–134, AGU, Washington, D. C.

Déry, S. J., and L. B. Tremblay (2004), Modeling the effects of wind redistribution on the snow mass budget of polar sea ice, *J. Phys. Oceanogr.*, *34*, 258–271, doi:10.1175/1520-0485(2004)034<0258:MTEOWR>2.0.CO;2.

Déry, S. J., and M. K. Yau (2002), Large-scale mass balance effects of blowing snow and surface sublimation, *J. Geophys. Res.*, *107*(D23), 4679, doi:10.1029/2001JD001251.

Déry, S. J., P. A. Taylor, and J. Xiao (1998), The thermodynamic effects of sublimating, blowing snow in the atmospheric boundary layer, *Boundary Layer Meteorol.*, *89*, 251–283, doi:10.1023/A:1001712111718.

Duda, D. P., J. D. Spinhirne, and E. W. Eloranta (2001), Atmospheric multiple scattering effects on GLAS altimetry. Part I: Calculations of single pulse bias, *IEEE Trans. Geosci. Remote Sens.*, *39*, 92–101, doi:10.1109/36.898668.

Fahnestock, M. A., T. A. Scambos, C. A. Shuman, R. J. Arthern, D. P. Winebrenner, and R. Kwok (2000), Snow megadune fields on the East Antarctic Plateau: Extreme atmosphere-ice interaction, *Geophys. Res. Lett.*, *27*, 3719–3722, doi:10.1029/1999GL011248.

Gallée, H., G. Guyomarc'h, and E. Brun (2001), Impact of snow drift on the Antarctic Ice Sheet surface mass balance: Possible sensitivity to snow-surface properties, *Boundary Layer Meteorol.*, *99*, 1–19, doi:10.1023/A:1018776422809.

Gordon, M., and P. A. Taylor (2009), Measurements of blowing snow, Part I: Particle shape, size distribution, velocity, and number flux at Churchill, Manitoba, Canada, *Cold Reg. Sci. Technol.*, *55*, 63–74, doi:10.1016/j.coldregions.2008.05.001.

Harder, S. L., S. G. Warren, R. J. Charlson, and D. S. Covert (1996), Filtering of air through snow as a mechanism for aerosol deposition to the Antarctic ice sheet, *J. Geophys. Res.*, *101*, 18,729–18,743, doi:10.1029/96JD01174.

King, J. C., P. S. Anderson, D. G. Vaughan, G. W. Mann, and S. D. Mobbs (2004), Wind-borne redistribution of snow across an Antarctic ice rise, *J. Geophys. Res.*, *109*, D11104, doi:10.1029/2003JD004361.

Lawson, R. P., B. A. Baker, P. Zmarzly, D. O'Connor, Q. Mo, J.-F. Gayet, and V. Shcherbakov (2006), Microphysical and optical properties of ice crystals at South Pole Station, *J. Appl. Meteorol.*, *45*, 1505–1524, doi:10.1175/JAM2421.1.

Lenaerts, J. T. M., M. R. van den, Broeke S. J. Déry, G. König-Langlo, J. Ettema, and P. K. Munneke (2010), Modelling snowdrift sublimation on an Antarctic ice shelf, *The Cryosphere*, *4*, 179–190, doi:10.5194/tc-4-179-2010.

Leonard, K. C., and T. Maksym (2011), The importance of wind-blown snow redistribution to snow accumulation on Bellinghausen Sea ice, *Ann. Glaciol.*, *52*(57), 271–278.

Leonard, K. C., L. B. Tremblay, D. R. MacAyealand, and S. S. Jacobs (2008), Interactions of wind-transported snow with a rift in the Ross Ice Shelf, Antarctica, *Geophys. Res. Lett.*, *35*, L05501, doi:10.1029/2007GL033005.

Lesins, G., L. Bourdages, T. J. Duck, J. R. Drummond, E. W. Eloranta, and V. P. Walden (2009), Large surface radiative forcing from topographic blowing snow residuals measured in the High Arctic at Eureka, *Atmos. Chem. Phys.*, *9*, 1847–1862, doi:10.5194/acp-9-1847-2009.

Li, L., and J. W. Pomeroy (1997), Estimates of threshold wind speeds for snow transport using meteorological data, *J. Appl. Meteorol.*, *36*, 205–213, doi:10.1175/1520-0450(1997)036<0205:EOTWSF>2.0.CO;2.

Mahesh, A., J. D. Spinhirne, D. P. Duda, and E. W. Eloranta (2002), Atmospheric multiple scattering effects on GLAS altimetry. Part II: Analysis of expected errors in Antarctic altitude measurements, *IEEE Trans. Geosci. Remote Sens.*, *40*, 2353–2362, doi:10.1109/TGRS.2002.803849.

Mahesh, A., R. Eager, J. R. Campbell, and J. D. Spinhirne (2003), Observations of blowing snow at the South Pole, *J. Geophys. Res.*, *108*(D22), 4707, doi:10.1029/2002JD003327.

Mann, G. W., P. S. Anderson, and S. D. Mobbs (2000), Profile measurements of blowing snow at Hallet, Antarctica, *J. Geophys. Res.*, *105*, 24,491–24,508, doi:10.1029/2000JD900247.

Monaghan, A. J., D. H. Bromwich, J. G. Powers, and K. W. Manning (2005), The climate of the McMurdo, Antarctica, Region as represented by one year of forecasts from the Antarctic Mesoscale Prediction System, *J. Clim.*, *18*, 1174–1189, doi:10.1175/JCLI3336.1.

Nishimura, K., and M. Nemoto (2005), Blowing snow at Mizuho station, Antarctica, *Philos. Trans. R. Soc. A*, *363*, 1647–1662, doi:10.1098/rsta.2005.1599.

Palm, S. P., J. D. Spinhirne, W. D. Hart, and D. L. Hlavka (2002), GLAS atmospheric data products, algorithm theoretical basis document, version 4.2, Goddard Space Flight Cent., Greenbelt, Md. (Available at http://www.csr.utexas.edu/glas/pdf/glasatmos.atbdv4.2.pdf.)

Palm, S. P., A. Benedetti, and J. Spinhirne (2005), Validation of ECMWF global forecast model parameters using GLAS atmospheric channel measurements, *Geophys. Res. Lett.*, *32*, L22S09, doi:10.1029/2005GL023535.

Picciotto, E. E., W. De Breuck, and G. Crozaz et al. (1970), Snow accumulation along the South Pole–Dronning Maud Land Traverse, in *International Symposium on Antarctic Glaciological Exploration*, edited by A. J. Gow et al., *IAHS Publ. 86*, 18–22.

Pomeroy, J. W., and R. L. H. Essery (1999), Turbulent fluxes during blowing snow: Field tests of model sublimation predictions, *Hydrol. Processes*, *13*, 2963–2975, doi:10.1002/(SICI)1099-1085(19991230)13:18<2963::AID-HYP11>3.0.CO;2-9.

Powers, J. G., A. J. Monaghan, A. M. Cayette, D. H. Bromwich, Y.-H. Kuo, and K. W. Manning (2003), Real-time mesoscale modeling over Antarctica: The Antarctic Mesoscale Prediction System, *Bull. Am. Meteorol. Soc.*, *84*, 1533–1545, doi:10.1175/BAMS-84-11-1533.

Renfrew, I. A., and G. W. K. Moore (1999), An extreme cold-air outbreak over the Labrador Sea: Roll vortices and air-sea interactions, *Mon. Weather Rev.*, *127*, 2379–2394, doi:10.1175/1520-0493(1999)127<2379:AECAOO>2.0.CO;2.

Scarchilli, C., M. M. Frezzotti, P. Grigioni, L. De Silvestri, L. Agnoletto, and S. Dolci (2010), Extraordinary blowing snow transport events in East Antarctica, *Clim. Dyn.*, *34*, 1195–1206, doi:10.1007/s00382-009-0601-0.

Schmidt, R. A. (1982), Properties of blowing snow, *Rev. Geophys.*, *20*, 39–44, doi:10.1029/RG020i001p00039.

Spinhirne, J. D., S. P. Palm, W. D. Hart, D. L. Hlavka, and E. J. Welton (2005), Cloud and aerosol measurements from GLAS: Overview and initial results, *Geophys. Res. Lett.*, *32*, L22S03, doi:10.1029/2005GL023507.

Stephens, G., et al. (2002), The CloudSat mission and the A-train, *Bull. Am. Meteorol. Soc.*, *83*, 1771–1790, doi:10.1175/BAMS-83-12-1771.

van de Berg, W. J., M. R. van Den Broeke, and E. van Meijgaard (2006), Reassessment of the Antarctic surface mass balance using calibrated output of a regional atmospheric climate model, *J. Geophys. Res.*, *111*, D11104, doi:10.1029/2005JD006495.

van den Broeke, M., W. J. van de Berg, E. van Meijgaard, and C. Reijmer (2006), Identification of Antarctic ablation areas using a regional atmospheric climate model, *J. Geophys. Res.*, *111*, D18110, doi:10.1029/2006JD007127.

Walden, V. P., S. Warren, and E. Tuttle (2003), Atmospheric ice crystals over the Antarctic Plateau in winter, *J. Appl. Meteorol.*, *42*, 1391–1405.

Whiteman, D. N., B. Demoz, and Z. Wang (2004), Subtropical cirrus cloud extinction to backscatter ratios measured by Raman Lidar during CAMEX-3, *Geophys. Res. Lett.*, *31*, L12105, doi:10.1029/2004GL020003.

Winker, D. M., W. H. Hunt, and M. J. McGill (2007), Initial performance assessment of CALIOP, *Geophys. Res. Lett.*, *34*, L19803, doi:10.1029/2007GL030135.

Winker, D. M., M. A. Vaughan, A. Omar, Y. Hu, K. A. Powell, Z. Liu, W. H. Hunt, and S. A. Young (2009), Overview of the CALIPSO Mission and CALIOP Data Processing Algorithms, *J. Atmos. Oceanic Technol.*, *26*, 2310–2323, doi:10.1175/2009JTECHA1281.1.

Xiao, J., R. Bintanja, S. J. Déry, G. W. Mann, and P. A. Taylor (2000), An intercomparison among four models of blowing snow, *Boundary Layer Meteorol.*, *97*, 109–135, doi:10.1023/A:1002795531073.

Yamanouchi, T., and S. Kawaguchi (1985), Effects of drifting snow on surface radiation budget in the katabatic wind zone, Antarctica, *Ann. Glaciol.*, *6*, 238–241.

Yang, Y., A. Marshak, T. Varnai, W. J. Wiscombe, and P. Yang (2010), Uncertainties in ice sheet altimetry measurements from a space-borne 1064 nm single channel lidar due to undetected thin clouds, *IEEE Trans. Geosci. Remote Sens.*, *48*, 250–259, doi:10.1109/TGRS.2009.2028335.

Yorks, J. E., M. McGill, D. Hlavka, and W. Hart (2011), Statistics of cloud optical properties from airborne lidar measurements, *J. Atmos. Oceanic Technol.*, doi:10.1175/2011JTECHA1507.1, in press.

A. Marshak, Goddard Space Flight Center, Mail Code 613.2, Greenbelt, MD 20771, USA.

S. P. Palm, Science Systems and Applications, Inc., Goddard Space Flight Center, Code 613.1, Greenbelt, MD 20771, USA. (stephen.p.palm@nasa.gov)

J. D. Spinhirne, Department of Electrical and Computer Engineering, University of Arizona, Bldg. 104, 1230 E. Speedway Blvd., Tucson, AZ 85721, USA.

Y. Yang, Universities Space Research Association, 10211 Wincopin Circle, Suite 500, Columbia, MD 21044, USA.